
MolEvolve: LLM-Guided Evolutionary Search for Interpretable Molecular Optimization

Xiangsen Chen¹ Ruilong Wu² Yanyan Lan³ Ting Ma⁴ Yang Liu¹

Abstract

Despite deep learning’s success in chemistry, its impact is hindered by a lack of interpretability and an inability to resolve ‘activity cliffs’, where minor structural nuances trigger drastic property shifts. Current representation learning, bound by the similarity principle, often fails to capture these structural-activity discontinuities. To address this, we introduce MolEvolve, an evolutionary framework that reformulates molecular discovery as an autonomous, look-ahead planning problem. Unlike traditional methods that depend on human-engineered features or rigid prior knowledge, MolEvolve leverages a Large Language Model (LLM) to actively explore and evolve a library of executable chemical symbolic operations. By utilizing the LLM to cold start and an Monte Carlo Tree Search (MCTS) engine for test-time planning with external tools (e.g. RD-Kit), the system self-discovers optimal trajectories autonomously. This process evolves transparent reasoning chains that translate complex structural transformations into actionable, human-readable chemical insights. Experimental results demonstrate that MolEvolve’s autonomous search not only evolves transparent, human-readable chemical insights, but also outperforms baselines in both property prediction and molecule optimization tasks.

1. Introduction

Deep learning has become a paradigm shift in molecule-related tasks from manual experimentation to data-centric discovery. In this domain, deep learning models, especially Graph Neural Networks (GNNs), have demonstrated remarkable performance by modeling the geometric topology

of molecules (Stärk et al., 2022; Li et al., 2023). Techniques such as pre-training on molecular data (e.g., atoms and bonds) have further solidified GNNs as the standard for diverse property prediction tasks (Stuyver & Coley, 2022; Cremer et al., 2023). More recently, Large Language Models (LLMs) show great promise in scientific tasks. Domain-specific LLMs (Taylor et al., 2022; Liu et al., 2024) and Retrieval-Augmented Generation (RAG) methods (Xian et al., 2025; Zhang et al., 2025) leverage parametric domain knowledge and vast corpora of external literature to capture knowledge and semantic understanding that deep learning models may miss.

In spite of their capabilities, these existing methods face significant limitations. Deep learning models like GNNs operate as black boxes despite their powerful capabilities in molecular data mining (Li et al., 2023; Lavecchia, 2025; Stegmann et al., 2023). They are often unable to provide accurate feature attributions to explain which specific substructures contribute to a given molecular property. This reduces the scientific interpretability of the models. In addition, GNN-based explanations (e.g., attention weights) serve as post-hoc approximations rather than intrinsic logic (Stegmann et al., 2023; He et al., 2024). On the other hand, LLMs, even when fine-tuned on domain-specific knowledge, are prone to hallucination (Suzgun et al., 2025). LLMs are prone to generate plausible but factually incorrect scientific knowledge or properties (Truhn et al., 2023), and they often struggle to predict accurate quantitative results (Wang et al., 2025).

Previous approaches often treat predictive precision and interpretability as separate objectives (Oviedo et al., 2022). Consequently, a critical gap remains: scientists need to know not just the final results, but the explicit causal rules that enable a molecule to possess a certain property (Mengaldo, 2024). We argue that the difficulty in achieving such interpretable precision arises from a fundamental representation-precision paradox. As demonstrated in Appendix B and Figure 1, molecular properties often exhibit high Lipschitz constants, known as ‘‘activity cliffs,’’ where minor structural nuances trigger drastic property shifts. This challenge arises from the severe topological mismatch between molecular manifolds and continuous semantic manifolds. Recent work

¹Hong Kong Polytechnic University ²Hong Kong University of Science and Technology(Guangzhou) ³Tsinghua University ⁴Harbin Institute of Technology (Shenzhen). Correspondence to: <yang-veronica.liu@polyu.edu.hk>.

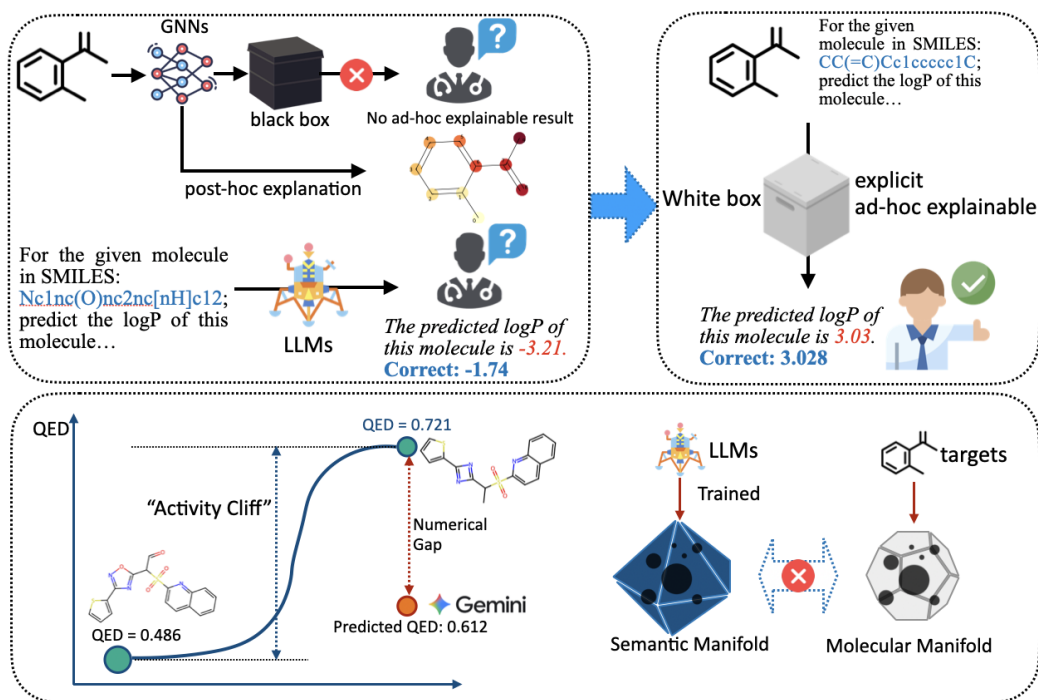


Figure 1. (Up) Existing GNNs act as black boxes with post-hoc interpretations, while LLMs suffer from numerical hallucinations on semantic manifolds. (Down) The representation-precision paradox: minor structural distances lead to "activity cliffs" in molecular manifolds, which LLMs fail to capture precisely due to semantic smoothing.

suggests that LLM internal representations are best characterized as manifolds where proximity reflects semantic similarity, rather than the precise Euclidean distances required for physical properties (Modell et al., 2025). LLMs attempt to map discrete chemical tokens onto continuous physical manifolds, which causes them to struggle with precise quantitative tasks (Wang et al., 2025; Truhn et al., 2023). While GNNs can fit these manifolds, their reasoning remains an opaque black box (Stegmann et al., 2023). To resolve this paradox, we argue that one must transcend continuous embeddings and operate within a space of executable symbolic logic. Unlike smooth vectors, discrete symbolic rules can naturally model non-linear discontinuities (e.g., logic branches). A fundamental missing piece is a mechanism to actively search for and verify explicit chemical rules, thereby transforming chemical feature engineering into a dynamic, goal-directed reasoning task.

To address the challenge, we propose the MolEvolve framework. Unlike simulations of fine-tuned LLMs or opaque GNN approximations, MolEvolve reformulates molecular discovery as explicit look-ahead planning over a space of executable chemical symbolic operations. Instead of outputting a final answer directly, the system actively constructs an explicit path. First, the framework initiates with an LLM-based cold start. It functions as a computational chemist to diagnose the molecule and propose initial heuristic rules (e.g., logP for solubility calculation). It distills symbolic

priors to seed the search. Then, we apply external chemical tools to generate corresponding rules. These rules serve as the foundation for our initialized MCTS search tree. The MCTS tree navigates the vast space of executable chemical rules guided by an LLM that proposes candidate operations for diverse downstream tasks (e.g. "adding a hydroxyl group" for optimization or "calculating the logP") with RDKit (Bento et al., 2020) as external tool. Crucially, we enforce a closed-loop verification mechanism: every proposed operation is rigorously evaluated by external tools during the search. This allows the model to discover the consequences of a rule and prune invalid or low-fidelity pathways before commitment. By grounding semantic reasoning in verifiable execution, our framework evolves transparent, high-precision chemical insights. We conduct quantitative experiments on different molecule-related tasks: property prediction and optimization. The results demonstrate that MolEvolve outperforms both GNNs and LLM-based methods in property prediction; We also show evidence that MolEvolve outperforms domain-specific models and vanilla strong LLMs.

Our main contributions are summarized as follows:

- We identify the challenge in achieving interpretable precision of molecular property, and propose MolEvolve to address it via test-time symbolic planning, bridging the gap between semantic intuition and physical rigor.

- We propose a closed-loop mechanism where an LLM acts as a molecule operator to iteratively evolve and refine chemical descriptors based on feedback.
- Extensive experiments on benchmarks demonstrate that our method outperforms specialized GNNs and general-purpose LLMs, while providing human-readable chemical insights.

2. Related Works

GNN for Molecules. GNNs have been developed to aggregate atomic features and bond interactions (Gilmer et al., 2020; Xu et al., 2018; Yang et al., 2021; Wang et al., 2022). Furthermore, pre-training strategies are capable of both learning representations from millions of molecular graphs (Zhou et al., 2023; Hu et al., 2019; Rong et al., 2020) and increasing performance in data-scarce scenarios (Gao et al., 2024). Despite their success in benchmarks (Wu et al., 2018; Van Tilborg et al., 2022), the inherent opacity of GNNs remains a significant problem in explainability. While recent efforts attempt to elucidate GNN decisions via subgraph and fragment identification (Panapitiya et al., 2024), attention mechanisms (Li et al., 2023), or attribution generation (Chen et al., 2025a; He et al., 2024), these explanations are predominantly post-hoc approximations (Ying et al., 2019). In addition, the GNN models will over-smooth out the small structural difference during information aggregation. They face a critical challenge known as "activity cliffs" (Van Tilborg et al., 2022). To mitigate this, recent works have focused on refining continuous representations on contrastive learning (Zhang et al., 2024; Shen et al., 2023), multi-grained perception (Shu et al., 2025) and weighted graphs (Chen et al., 2025b). Despite these advances, these methods predominantly focus on patching the continuous embedding space. However, they remain constrained by the underlying message-passing paradigm, where small structural differences are inevitably over-smoothed out during information aggregation.

LLMs for Molecules. The success of LLMs has catalyzed a surge of interest in adapting them for scientific domains. In order to make LLMs understand molecules, early works focused on treating molecular strings as language (Weininger, 1988; Krenn et al., 2022). With this, fine-tuned LLMs are applied (Raffel et al., 2020; Touvron et al., 2023) for molecule generation and property prediction (Taylor et al., 2022; Liu et al., 2024; Wu et al., 2025a). More recently, the paradigm has shifted towards LLM agents that utilize external tools. These agents, like ChemCrow (Bran et al., 2023) empower LLMs in chemical sciences by multi-agent collaboration or invoking chemistry-related scripts or APIs (Wu et al., 2025b; Ghafarollahi & Buehler, 2025). To mitigate the lack of domain knowledge, RAG-based methods (Xian et al.,

2025; Zhang et al., 2025) integrate external scientific literature into the LLM’s context window to enhance reasoning capabilities. However, as highlighted in Section 1, LLMs are prone to molecular numerical hallucinations because they rely on the continuous manifold assumption (Wang et al., 2025; Truhn et al., 2023). Existing works attempt to mitigate this by evolving from linear SMILES modeling to multi-view multi-modal frameworks (Ju et al., 2025). To mitigate hallucinations and enhance activity cliff estimation, recent works employ strategies from optimized prompting (Reed, 2025) to semi-supervised curriculum learning (Wu, 2024). In addition, frameworks seek to enrich molecular representations by using LLM-generated textual explanations to guide representation learning via contrastive objectives (Wang et al., 2024) or employing instruction tuning to align LLMs with molecular graph modalities (Yu et al., 2025). Despite these methodological advancements, these approaches predominantly focus on enhancing LLMs through adding views, tuning prompts, or augmenting data, without addressing the fundamental topological mismatch of the continuous embedding space.

3. Method

We demonstrate MolEvolve in this chapter. As illustrated in Figure 2, MolEvolve reframes molecular engineering as a directed search problem over an executable symbolic chemical space.

3.1. Cold-start for Symbolic Knowledge Distillation

Overview. Exploring the discrete and large molecular space presents a fundamental challenge for heuristic-free search algorithms. In particular, standard MCTS suffers from prohibitive sample complexity during its initialization phase due to the absence of effective guidance. To address this limitation, the cold start mechanism introduces informative priors. Rather than discovering chemical rules from scratch via trial-and-error, our approach explicitly encodes these rules into the search process. As illustrated in Figure 2, our cold start mechanism operates as a symbolic knowledge distillation process. It consists of three stages: (1) **Knowledge Synthesis**, where abstract chemical rules are analyzed by LLMs; (2) **Symbolic Grounding**, where rules are translated into executable code; and (3) **Iterative Self-Correction**, which ensures the validity of the generated logic through execution feedback.

Knowledge Synthesis. Directly asking an LLM to write code often yields incorrect or irrelevant functions. To mitigate this, we first employ CoT (Wei et al., 2022) prompting strategy to synthesize text-based prior knowledge. Given the task \mathcal{T} , we use task-specific prompt $\mathcal{P}_0(\mathcal{T})$ to identify critical molecular substructures or physicochemical properties associated with the target label. Formally, this step

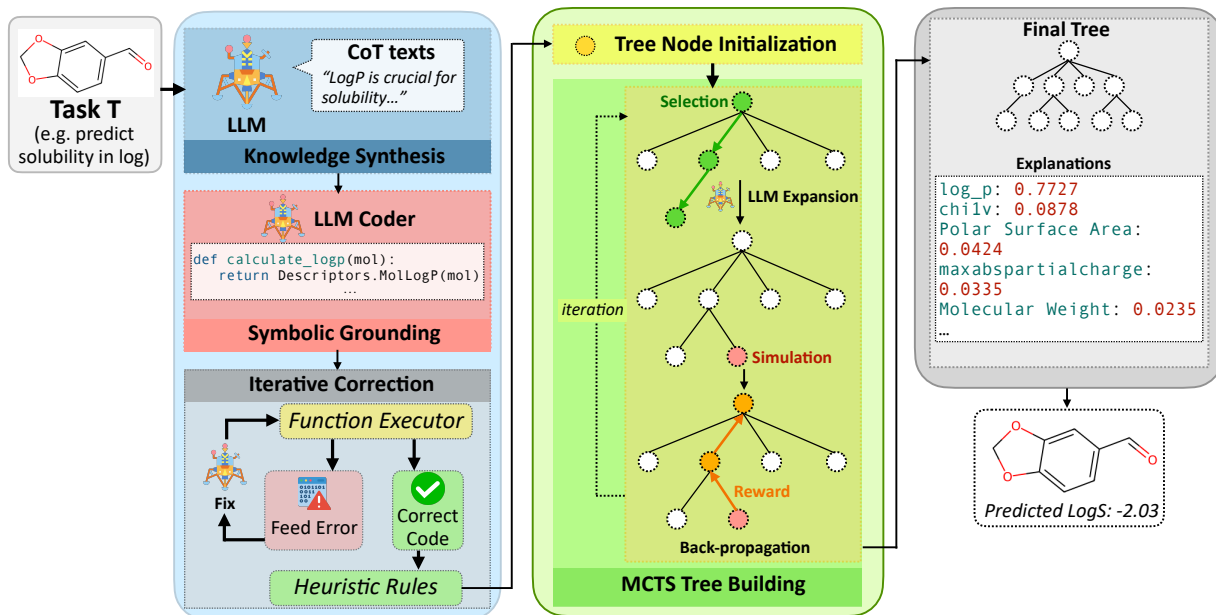


Figure 2. The overall architecture of MolEvolve. Phase 1 (Cold Start) distills domain knowledge into executable heuristic rules via symbolic grounding and self-correction. Phase 2 (LLM-MCTS) utilizes these rules to initialize an evolutionary search tree, where the LLM acts as molecule operator to guide selection and expansion within a rigorous verification loop.

produces a set of textual rules $\mathcal{K}_{text} = \text{LLM}(\mathcal{P}_0(\mathcal{T}))$. This textual representation ensures the subsequent code generation is grounded in chemical logic rather than mere syntax completion. An example can be viewed in Appendix E.

Symbolic Grounding via Code Generation. To make \mathcal{K}_{text} usable by MCTS, we must ground natural language into symbolic representations. Given a molecule SMILES string S , for each rule $\mathcal{K}_{text}^{(i)} \in \mathcal{K}_{text}$, we employ LLM as coder to translate it into Python function $\phi_i \in \Phi$ with standard chemical libraries like RDKit. We denote this as $\Phi = \{\phi_i = \text{LLM}(\mathcal{K}_{text}^{(i)})\}_{\mathcal{K}_{text}^{(i)} \in \mathcal{K}_{text}}$. This grounded representation Φ enables rigorous mathematical operations in the subsequent search process.

Execution-based Iterative Self-Correction. A critical challenge in LLM-based coding is the generation of non-executable buggy code. We propose a closed-loop self-correction mechanism. For each generated function ϕ_i , we attempt to execute it. If an exception occurs, we capture the error trace and feed it back to the LLM:

$$\phi_i^{t+1} \leftarrow \text{LLM}(\phi_i^t, e, \mathcal{P}_{fix}) \quad (1)$$

where \mathcal{P}_{fix} is a rectification prompt. This loop repeats until ϕ_i executes successfully or a retry limit is reached.

3.2. LLM-guided Evolutionary Search

To evolutionarily explore the chemical space, we adopt a modified MCTS framework that integrates symbolic knowledge distilled from the cold start phase. Unlike conventional MCTS approaches that rely on random rollouts or purely data-driven value networks, our framework leverages LLMs to guide the search process for ensuring both chemical validity and boosting search space. We define a search state s as a tuple of features \mathcal{F} (in molecule prediction) or a molecular SMILES string S (in molecular optimization). Importantly, the initial state s_0 is constructed with the symbolic functions Φ generated during the cold start phase, which provides an initialization with domain-specific inductive knowledge. Our MCTS follows the standard four-stage procedure: *Selection*, *Expansion*, *Simulation*, and *Backpropagation*. We introduce key modifications to the *Expansion* and *Simulation* stages to explicitly incorporate symbolic knowledge. A detailed formal comparison of detailed formulations of MCTS stage for tasks selected in our paper is provided in Appendix A (see Table 5).

Selection. We adopt the Upper Confidence Bound for Trees (UCT) strategy to traverse the tree from the root to a leaf node, balancing exploration and exploitation:

$$a_t = \arg \max_{a \in \mathcal{A}(s)} \left(Q(s, a) + c \cdot \sqrt{\frac{\ln N(s)}{N(s, a)}} \right), \quad (2)$$

where $Q(s, a)$ is the estimated value of action a in state s , $N(s)$ is the visit count of state s , $N(s, a)$ is the visit count of action a , and c is an exploration constant.

LLM-Guided Node Expansion. Instead of exhaustively enumerating all possible chemical modifications, we employ the LLM as a generative policy network conditioned on the symbolic priors. Given a leaf state s_L , the LLM is prompted with the textual rules \mathcal{K}_{text} derived in the cold start phase (e.g., specific structural liabilities or optimization directions) to propose a set of high-potential actions. This design ensures that the expansion is not a random exploration but a focused execution of the diagnostic logic established in cold start phase, thereby integrating the cold-start knowledge directly into the evolutionary search loop.

Simulation. Instead of performing deep Monte Carlo roll-outs which are computationally expensive, we immediately evaluate the expanded node using the composite reward function. The reward function integrates task-specific objectives with symbolic heuristic guidance from Φ . It consists of three distinct objectives: the primary task performance (R_{task}), the alignment with symbolic priors ($R_{heuristic}$), and structural constraints ($R_{penalty}$). The reward for a state s is defined as:

$$R(s) = R_{task}(s) + \lambda \cdot R_{heuristic}(s, \Phi) + \gamma \cdot R_{penalty}(s), \quad (3)$$

This composite reward formulation enables MCTS to navigate sparse reward landscapes by exploiting dense heuristic feedback provided by the cold start mechanism. $R_{task}(s)$ captures the primary task objective, such as validation performance (RMSE or AUC) for prediction tasks or molecular property scores (e.g., QED, LogP). $R_{heuristic}(s, \Phi)$ measures the symbolic alignment with the cold-start priors. We formulate this term as the cumulative execution score of the generated symbolic rules Φ in the cold start phase. For a set of symbolic functions $\Phi = \{\phi_1, \dots, \phi_k\}$, the alignment score is defined as the weighted sum of satisfied rules:

$$R_{heuristic}(s, \Phi) = \sum_{\phi_i \in \Phi} \mathbb{I}(\phi_i(s) = \text{True}), \quad (4)$$

where $\mathbb{I}(\cdot)$ is the indicator function, $\phi_i(s)$ represents the execution of the i -th Python rule generated by the LLM (e.g., checking for specific pharmacophores). $R_{penalty}(s)$ enforces constraints, such as penalizing low structural similarity to the initial molecule (to preserve the scaffold) or chemically invalid structures. λ and γ are hyperparameters that balance data-driven signals and symbolic priors.

Backpropagation. The computed reward $R(s)$ is propagated back through the search tree, updating the Q -values and visit counts of all ancestor nodes. This feedback mechanism allows the search to progressively concentrate on the most promising regions of the chemical space, as identified through the synergy between LLM reasoning and rigorous simulation.

4. Experiment

4.1. Experimental Settings

Datasets and Tasks. We evaluate MolEvolve on two fundamental molecular tasks: (1) **Property Prediction**, utilizing five benchmarks from MoleculeNet (Wu et al., 2018), including regression tasks (ESOL, Lipophilicity) and classification tasks (BACE, BBBP, HIV). (2) **Property Optimization**, using the ChemCoTBench (Li et al., 2025) benchmark to evaluate the model’s ability to improve molecular properties. Results are averaged over 3 independent runs. We follow (Guo et al., 2023) and split the dataset into an 80/10/10% for training, validation and test sets.

Baselines. We compare our approach against three categories of methods. **GNN-based Methods:** Specialized graph models including GIN (Xu et al., 2018) and Graphformer (Yang et al., 2021). **LLM Baselines:** Including RAG-based baselines, like Automolco (Zhang et al., 2025), MolRAG (Xian et al., 2025), and fine-tuned LLMs like Attrilens-mol (Lin et al., 2025). **Strong Reasoning Models:** Evaluation of the internal reasoning capabilities of proprietary and open-source LLMs.

Metrics. For property prediction tasks, we adopt Root Mean Square Error (RMSE) (lower value for better performance) for regression and ROC-AUC (higher value for better performance) for classification. For the property optimization task, we measure through two metrics: Improvement (Δ) and Success Rate (SR%). The Improvement metric calculates the average absolute increase in the target property achieved by the model starting from the initial molecule. The SR% represents the percentage of test cases where the model successfully generates a valid molecule with a property value higher than that of the starting molecule.

4.2. Main Results

Property Prediction. The results in Table 1 illustrate the predictive performance of MolEvolve across diverse tasks. MolEvolve consistently achieves a significant reduction in error rates for regression tasks. On the ESOL dataset, MolEvolve maintains an RMSE around 0.69, which is much lower than that of LLM-based baselines like MolRAG (Xian et al., 2025). Baselines suffer from numerical hallucinations due to the representation-precision paradox. Their reliance on semantic approximations over-smooths the molecular manifold, which may trigger giant bias in chemical manifolds. We resolve this by grounding executable code. By generating deterministic code rather than stochastic values, our framework ensures predictions adhere to deterministic chemical logic. Notably, MolEvolve with Qwen2.5-7B-Instruct outperforms GNNs such as Graphformer. This outcome indicates that the symbolic features discovered through search are more effective than high-dimensional black-box embed-

Table 1. Comparative results for molecular property prediction on MoleculeNet benchmarks. For regression tasks (ESOL, Lipophilicity), we report RMSE (lower is better). For classification tasks (BACE, BBBP, HIV), we report ROC-AUC (higher is better).

Base Model	Method	Regression (RMSE ↓)		Classification (ROC-AUC ↑)		
		ESOL	Lipo.	BACE	BBBP	HIV
Qwen2.5-7B-Instruct	Automolco (Zhang et al., 2025)	1.0566	1.0854	0.6716	0.6102	0.6265
	MolRAG (Xian et al., 2025)	1.7160	2.5412	0.6968	0.5608	0.6476
	ATTRILENS-MOL (Lin et al., 2025)	1.8420	-	0.6102	0.5810	-
	MolEvolve	0.6890	0.8527	0.7705	0.7461	0.7581
GPT-4o-mini	Automolco (Zhang et al., 2025)	1.0062	1.0630	0.7390	0.6435	0.6583
	MolRAG (Xian et al., 2025)	1.2355	1.7800	0.7762	0.6392	0.6823
	MolEvolve	0.6914	0.8055	0.7854	0.7268	0.7281
GPT-4o	Automolco (Zhang et al., 2025)	0.8538	1.0591	0.7310	0.6637	0.6750
	MolRAG (Xian et al., 2025)	1.4237	1.2967	0.7663	0.6271	0.6209
	MolEvolve	0.6869	0.8188	0.7875	0.7291	0.7682
GNNs	GIN (Xu et al., 2018)	1.2182	1.5481	0.7326	0.6953	0.7450
	Graphformer (Yang et al., 2021)	0.9260	1.2367	0.7695	0.7012	0.7788
Tree-based model	XGBoost	0.9364	0.9833	0.6428	0.6864	0.7020
	Decision Tree	0.8287	1.1135	0.6352	0.6037	0.5566
Linear model	Logistic Regression (LR)	0.9970	1.0651	0.6334	0.6727	0.6571

Table 2. Molecular property optimization results on ChemCoT-Bench. Improvement measures the average increase in target property, and SR% (Success Rate) measures the percentage of instances with property improvement. In MolEvolve, the **Base Model** column specifies the backbone LLM integrated within the architecture.

Base Model	LogP		QED	
	Δ	SR%	Δ	SR%
<i>MolEvolve (Ours)</i>				
GPT-4o-mini	1.925	85%	0.264	55%
Qwen2.5-7B-Instruct	1.271	63%	0.245	58%
Qwen2.5-32B-Instruct	2.126	82%	0.258	60%
<i>Baseline Models</i>				
GPT-5	0.257	53%	0.204	66%
Qwen3-235B-A22B-think	0.050	40%	0.020	24%
DeepSeek-R1	0.371	76%	0.074	71%
DeepSeek-V3	0.102	28%	0.090	46%
BioMistral-7B (Labrak et al., 2024)	-0.360	18%	-0.295	15%
BioMedGPT-7B (Luo et al., 2023)	0.012	2%	0.000	0%

dings. In classification tasks, our method also demonstrates strong performance on diverse datasets.

Property Optimization. Table 2 presents the performance of MolEvolve in molecular optimization tasks. Our method shows a substantial advantage over strong LLMs in the optimization tasks. For LogP optimization, MolEvolve achieves an improvement score nearly 4 times higher than that of DeepSeek-R1 with Qwen2.5-7B-Instruct as the base model. This significant gap reveals the limitations of implicit reasoning of LLMs. Reasoning LLMs, like DeepSeek-R1, rely on their internal thinking path. They lack the ability to backtrack from failed structural modifications in the

vast combinatorial chemical space. In contrast, our MCTS engine performs explicit lookahead planning. It systematically explores multiple search branches and verifies each step through external tools. A key observation is that our search-centric approach effectively bridges the capability gap between LLMs of different scales. With the full MCTS framework, the Qwen2.5-7B-Instruct ($\Delta = 1.271$ and Success Rate 63% on LogP) is able to outperform strong LLMs like GPT-5 and DeepSeek-V3. This result demonstrates that MolEvolve effectively transforms the optimization problem into a manageable evolutionary search process.

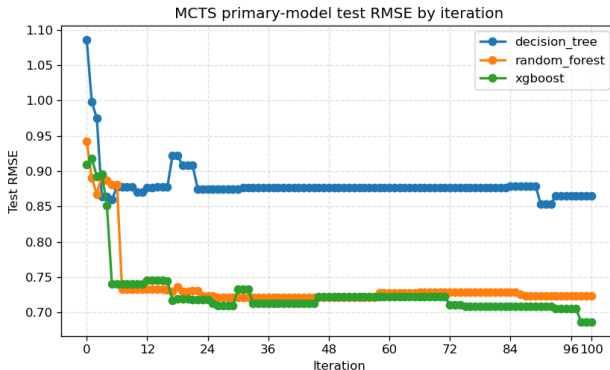


Figure 3. Search Efficiency and Model Adaptability Analysis: Test RMSE trajectories across 100 iterations. To verify that the evolved symbolic features are model-agnostic, we employ three distinct primary models as downstream evaluators. In each iteration, the MCTS engine generates a candidate feature set, which is then frozen to train these evaluators for scoring.

Analysis of Search Progress. To further investigate the effectiveness of the searching module of MolEvolve, we

visualize the evolutionary trajectories for both property prediction (Figure 3) and molecular optimization (Figure 4). The trajectories are across $T = 100$ and $T = 30$ MCTS iterations, respectively. The test set is held out and trajectory analyses report the performance of the optimized model on the held-out test set only after the search concludes. To demonstrate that the accumulated knowledge is model-agnostic, we employ Random Forest, XGBoost, and Decision Tree as primary evaluators in property prediction. The results of both tasks demonstrate a rapid initial convergence in the first steps, which is facilitated by the LLM-driven cold start, and distinct 'step-wise' improvements. It distills essential chemical priors into an initial set of executable rules, providing a high-quality starting manifold. For **Property Prediction**, the RMSE trajectory shows an exploration-breakthrough dynamic over 100 iterations. The initial plateau phase (e.g., iterations 20-90) corresponds to the MCTS engine navigating the combinatorial rule space (exploring ~ 30 candidates per step) to accumulate necessary feature precursors. Unlike greedy methods, MCTS tolerates this latency to identify synergistic combinations. The subsequent drop in RMSE signifies a synergistic breakthrough, where the interaction of a newly discovered feature with the accumulated set \mathcal{F} (typically $|\mathcal{F}| \approx 20$) successfully resolves the "activity cliff". The **Molecular Optimization** trajectory (Figure 4) displays a more rapid optimization pattern. All backbone LLMs exhibit a steep initial ascent, which confirms that distilled rules from Cold Start phase provide immediate, valid structural directives rather than random perturbations. Compared to property prediction task, convergence occurs early (~ 30 iterations) in molecular optimization. It indicates that constructive structural editing yields more direct feedback than the combinatorial feature discovery required for prediction.

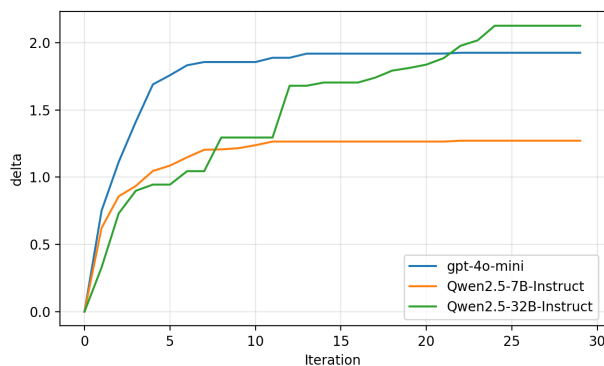


Figure 4. An Example of Evolutionary Trajectory of Molecular Optimization(logP).

Case Study of Real-Time Explanation. To address the theoretical challenge of "activity cliffs" and verify MolEvo's ability to navigate complex chemical manifolds, we analyze the optimization of property logP and QED (see

Figure 6 and Figure 7 of Appendix D for the detailed trace). First, we analyze the optimization of LogP (Figure 6). Initially, the cold-start phase identifies structural liabilities, and distills symbolic prescription. As illustrated in Figure 6, our MCTS engine systematically explores the structural space. Unlike proposing chemically invalid molecules or stuck in local optima, MolEvo employs the Function Executor to prune non-physical paths. The finalized molecule, CC=C1NC(C(C)C)C(=O)N(C)C1Cc1ccc(OC)cc1C, demonstrates a drastic improvement of $\Delta\text{LogP} = 3.60$, nearly 5 times higher than the improvement achieved by deep-reasoning LLMs like DeepSeek-R1. This trajectory confirms that MolEvo follows chemical logic with real-time traceable interpretability. In addition, we examine the search trajectory for QED (Figure 7). Our MCTS engine employs explicit look-ahead planning that prevents stagnating in the local optima. As demonstrated in the trace, the search initially enters a sub-optimal branch. Then it executes a backpropagation to the parent node and identifies a synergistic replacement (Nitro \rightarrow Isopropyl). This symbolic edit successfully resolving the property bottleneck (QED \rightarrow 0.831), demonstrating it triggers the "activity cliff". This case reinforces our central claim again that, by grounding reasoning in an executable search tree, MolEvo effectively decouples physical precision from semantic smoothness and offers *real-time interpretability* that every structural edit corresponds to a specific heuristic rule, and creating a transparent trail for chemists.

4.3. Ablation Studies

Necessity of Cold Start and Evolutionary Search. The comprehensive ablation studies (Table 3 and Table 4) demonstrate substantial performance gains of different modules across both property prediction and optimization tasks. A full analysis of each benchmark is demonstrated in Appendix C. Vanilla LLMs consistently struggle across both prediction and optimization tasks, which fall short in the *representation-precision paradox*. The integration of the Cold Start phase effectively mitigates this by anchoring the model with domain-specific symbolic priors, transforming stochastic hallucinations into deterministic, executable calculations. However, the most profound performance gains are driven by the Full MCTS framework. The results indicate that while Cold Start phase provides a high-quality starting manifold, they are insufficient on their own. Navigating the combinatorial chemical space requires the MCTS engine's capacity for explicit look-ahead planning and backtracking. Ultimately, MolEvo succeeds by decoupling physical precision from semantic generation, which is governed by verifiable evolutionary search rather than random sampling.

Analysis of Hyperparameters. To understand the relationship between symbolic reasoning and structural exploration,

Table 3. Ablation study for molecular property prediction.

Module	RMSE ↓		ROC-AUC ↑		
	ESOL	Lipo	BACE	BBBP	HIV
<i>Base Model: Qwen2.5-7B-Instruct</i>					
Vanilla LLM	1.984	2.251	0.590	0.377	0.621
w/o Cold Start + MCTS	0.831	0.959	0.671	0.691	0.702
w. cold start + MCTS	0.689	0.853	0.771	0.746	0.758
<i>Base Model: GPT-4o-mini</i>					
Vanilla LLM	1.873	1.763	0.702	0.443	0.677
w/o Cold Start + MCTS	0.820	0.922	0.739	0.678	0.689
w. cold start + MCTS	0.691	0.806	0.785	0.727	0.728
<i>Base Model: GPT-4o</i>					
Vanilla LLM	1.830	1.524	0.489	0.499	0.514
w/o Cold Start + MCTS	0.737	0.882	0.750	0.681	0.714
w. cold start + MCTS	0.687	0.819	0.788	0.729	0.768

Table 4. Ablation study on ChemCoTBench optimization task. Δ and SR% represent the average property improvement and success rate, respectively.

Modules	LogP		QED	
	Δ	SR%	Δ	SR%
<i>Base Model: GPT-4o-mini</i>				
Vanilla LLM	0.148	24%	0.186	31%
+ Cold Start	0.780	42%	0.254	36%
+ Full MCTS	1.925	85%	0.264	55%
<i>Base Model: Qwen2.5-7B-Instruct</i>				
Vanilla LLM	-0.662	11%	0.146	28%
+ Cold Start	-0.551	13%	0.178	35%
+ Full MCTS	1.271	63%	0.245	58%
<i>Base Model: Qwen2.5-32B-Instruct</i>				
Vanilla LLM	-0.032	17%	0.024	15%
+ Cold Start	0.031	37%	0.138	51%
+ Full MCTS	2.126	82%	0.258	60%

we conduct a sensitivity analysis on the two key hyperparameters governing the reward function: the **heuristic guidance weight** (λ), which scales the influence of LLM-generated symbolic priors, and the **similarity penalty weight** (γ), which penalizes the structural deviation from the source scaffold. The results for LogP and QED optimization are presented in Figure 5. We observe a distinct convex trend across both tasks as λ increases. At low λ values, the system degenerates into a quasi-random search, which lacking the high-level planning required to navigate complex chemical spaces. Conversely, an excessively high λ forces the MCTS to rigidly adhere to LLM-generated heuristics. This effectively suppresses the capability, reducing the system to a greedy follower of the LLM’s potentially hallucinated advice. Overall, the optimal strategy is a synergy where the LLM provides broad strategic direction, while the MCTS engine retains sufficient autonomy to verify and refine these

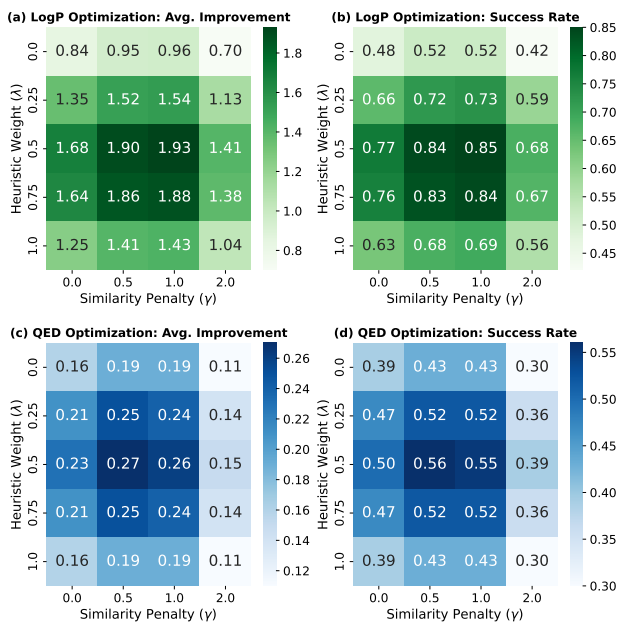


Figure 5. Hyperparameter Sensitivity Analysis Heatmaps. We visualize the Average Improvement (Left) and Success Rate (Right) for LogP (Top) and QED (Bottom) tasks. Darker colors indicate superior performance.

suggestions against physical reality. The similarity penalty γ acts as a regularizer to balance exploration and scaffold preservation. Without this penalty, the model tends to make trivial modifications that preserve the scaffold, but fail to trigger "activity cliff". However, this is a trade-off; an aggressive penalty ($\gamma = 2.0$) imposes an excessive cost on structural modifications, and causes a sharp drop in success rate. Interestingly, QED optimization task favors a slightly less constraint compared to LogP optimization task. This phenomenon can be attributed to reflecting the higher sensitivity of drug-likeness scores to more drastic structural modifications.

5. Conclusion

We introduce MolEvolve that reformulates molecular optimization as a dynamic search over an explicit, executable symbolic space. By distilling chemical priors via a cold-start mechanism and rigorously verifying evolved rules through a closed-loop search engine, our approach effectively bridges the gap between the semantic manifold of LLMs and the manifold of molecular properties. Empirical results across property prediction and optimization tasks demonstrate that MolEvolve not only outperforms baselines but also provides human-readable chemical insights. This shift from implicit neural representations to explicit symbolic evolution offers a new way for scientific discovery. Future work will extend this paradigm to multi-objective AI drug design and explore the integration of laboratory automation.

Impact Statement

This paper highlights that our proposed MolEvolve effectively addresses the Representation-Precision Paradox in AI-driven automated molecular discovery. By leveraging the symbolic priors and MCTS look-ahead planning, MolEvolve outperforms existing black-box deep learning paradigms with transparent, human-readable reasoning chains. This shift from implicit continuous fitting to explicit symbolic operations fosters greater trust in AI-assisted decision-making.

References

- Bento, A. P., Hersey, A., Félix, E., Landrum, G., Gaulton, A., Atkinson, F., Bellis, L. J., De Veij, M., and Leach, A. R. An open source chemical structure curation pipeline using rdkit. *Journal of Cheminformatics*, 12(1):51, 2020.
- Bran, A. M., Cox, S., Schilter, O., Baldassari, C., White, A. D., and Schwaller, P. Chemcrow: Augmenting large-language models with chemistry tools. *arXiv preprint arXiv:2304.05376*, 2023.
- Chen, X., Yu, D., Zhao, L., and Liu, F. Aces-gnn: Can graph neural network learn to explain activity cliffs? *Digital Discovery*, 2025a.
- Chen, Y., Wu, T., Jiang, Y., Nie, L., Li, G., Zhang, Y., Zhou, Z., Xu, J., Quan, L., and Lyu, Q. Mapcliff-wmgr: Exploring activity cliffs in molecular activity prediction enhanced by weighted molecular graph representations. *Journal of Chemical Information and Modeling*, 65(23): 12978–12989, 2025b.
- Cremer, J., Medrano Sandonas, L., Tkatchenko, A., Clevert, D.-A., and De Fabritiis, G. Equivariant graph neural networks for toxicity prediction. *Chemical Research in Toxicology*, 36(10):1561–1573, 2023.
- Gao, Q., Dukker, T., Schweidtmann, A. M., and Weber, J. M. Self-supervised graph neural networks for polymer property prediction. *Molecular Systems Design & Engineering*, 9(11):1130–1143, 2024.
- Ghafariollahi, A. and Buehler, M. J. Sciagents: automating scientific discovery through bioinspired multi-agent intelligent graph reasoning. *Advanced Materials*, 37(22): 2413523, 2025.
- Gilmer, J., Schoenholz, S. S., Riley, P. F., Vinyals, O., and Dahl, G. E. Message passing neural networks. In *Machine learning meets quantum physics*, pp. 199–214. Springer, 2020.
- Guo, T., Nan, B., Liang, Z., Guo, Z., Chawla, N., Wiest, O., Zhang, X., et al. What can large language models do in chemistry? a comprehensive benchmark on eight tasks. *Advances in Neural Information Processing Systems*, 36: 59662–59688, 2023.
- He, Y., Zheng, Z., Soga, P., Zhu, Y., Li, J., et al. Explaining graph neural networks with large language models: A counterfactual perspective for molecular property prediction. *arXiv preprint arXiv:2410.15165*, 2024.
- Hu, W., Liu, B., Gomes, J., Zitnik, M., Liang, P., Pande, V., and Leskovec, J. Strategies for pre-training graph neural networks. *arXiv preprint arXiv:1905.12265*, 2019.
- Ju, J., Zheng, Y., Koh, H. Y., Wang, C., and Pan, S. M²llm: Multi-view molecular representation learning with large language models. *arXiv*, 2025.
- Krenn, M., Ai, Q., Barthel, S., Carson, N., Frei, A., Frey, N. C., Friederich, P., Gaudin, T., Gayle, A. A., Jablonka, K. M., et al. Selfies and the future of molecular string representations. *Patterns*, 3(10), 2022.
- Labrak, Y., Bazoge, A., Morin, E., Gourraud, P.-A., Rouvier, M., and Dufour, R. Biomistral: A collection of open-source pretrained large language models for medical domains. *arXiv preprint arXiv:2402.10373*, 2024.
- Lavecchia, A. Explainable artificial intelligence in drug discovery: bridging predictive power and mechanistic insight. *Wiley Interdisciplinary Reviews: Computational Molecular Science*, 15(5):e70049, 2025.
- Li, H., Cao, H., Feng, B., Shao, Y., Tang, X., Yan, Z., Yuan, L., Tian, Y., and Li, Y. Beyond chemical qa: Evaluating llm’s chemical reasoning with modular chemical operations. *arXiv preprint arXiv:2505.21318*, 2025.
- Li, Y., Hostallero, D. E., and Emad, A. Interpretable deep learning architectures for improving drug response prediction performance: myth or reality? *Bioinformatics*, 39(6):btad390, 2023.
- Lin, X., Chen, L., and Wang, Y. Attrilens-mol: Attribute guided reinforcement learning for molecular property prediction with large language models. *arXiv preprint arXiv:2508.04748*, 2025.
- Liu, Y., Ding, S., Zhou, S., Fan, W., and Tan, Q. Moleculargpt: Open large language model (llm) for few-shot molecular property prediction. *arXiv preprint arXiv:2406.12950*, 2024.
- Luo, Y., Zhang, J., Fan, S., Yang, K., Wu, Y., Qiao, M., and Nie, Z. Biomedgpt: Open multimodal generative pre-trained transformer for biomedicine. *arXiv preprint arXiv:2308.09442*, 2023.

- Mengaldo, G. Explain the black box for the sake of science: the scientific method in the era of generative artificial intelligence. *arXiv preprint arXiv:2406.10557*, 2024.
- Modell, A., Rubin-Delanchy, P., and Whiteley, N. The origins of representation manifolds in large language models. *arXiv preprint arXiv:2505.18235*, 2025.
- Oviedo, F., Ferres, J. L., Buonassisi, T., and Butler, K. T. Interpretable and explainable machine learning for materials science and chemistry. *Accounts of Materials Research*, 3(6):597–607, 2022.
- Panapitiya, G., Gao, P., Maupin, C. M., and Saldanha, E. G. Fragnet: A graph neural network for molecular property prediction with four levels of interpretability. *arXiv preprint arXiv:2410.12156*, 2024.
- Raffel, C., Shazeer, N., Roberts, A., Lee, K., Narang, S., Matena, M., Zhou, Y., Li, W., and Liu, P. J. Exploring the limits of transfer learning with a unified text-to-text transformer. *Journal of machine learning research*, 21 (140):1–67, 2020.
- Reed, S. M. Augmented and programmatically optimized llm prompts reduce chemical hallucinations. *Journal of Chemical Information and Modeling*, 65(9):4274–4280, 2025.
- Rong, Y., Bian, Y., Xu, T., Xie, W., Wei, Y., Huang, W., and Huang, J. Self-supervised graph transformer on large-scale molecular data. *Advances in neural information processing systems*, 33:12559–12571, 2020.
- Shen, W. X., Cui, C., Shi, X. C., Zhang, Y. B., Wu, J., and Chen, Y. Z. Online triplet contrastive learning enables efficient cliff awareness in molecular activity prediction. 2023.
- Shu, Z., Deng, Y., Zhang, H., Nie, Z., and Chen, J. Mtpnet: Multi-grained target perception for unified activity cliff prediction. *arXiv preprint arXiv:2506.05427*, 2025.
- Stärk, H., Beaini, D., Corso, G., Tossou, P., Dallago, C., Günemann, S., and Liò, P. 3d infomax improves gnns for molecular property prediction. In *International Conference on Machine Learning*, pp. 20479–20502. PMLR, 2022.
- Stegmann, J.-U., Littlebury, R., Trengove, M., Goetz, L., Bate, A., and Branson, K. M. Trustworthy ai for safe medicines. *Nature Reviews Drug Discovery*, 22(10):855–856, 2023.
- Stuyver, T. and Coley, C. W. Quantum chemistry-augmented neural networks for reactivity prediction: Performance, generalizability, and explainability. *The Journal of Chemical Physics*, 156(8), 2022.
- Suzgun, M., Gur, T., Bianchi, F., Ho, D. E., Icard, T., Jurafsky, D., and Zou, J. Language models cannot reliably distinguish belief from knowledge and fact. *Nature Machine Intelligence*, pp. 1–11, 2025.
- Taylor, R., Kardas, M., Cucurull, G., Scialom, T., Hartshorn, A., Saravia, E., Poulton, A., Kerkez, V., and Stojnic, R. Galactica: A large language model for science. *arXiv preprint arXiv:2211.09085*, 2022.
- Touvron, H., Lavril, T., Izacard, G., Martinet, X., Lachaux, M.-A., Lacroix, T., Rozière, B., Goyal, N., Hambro, E., Azhar, F., et al. Llama: Open and efficient foundation language models. *arXiv preprint arXiv:2302.13971*, 2023.
- Truhn, D., Reis-Filho, J. S., and Kather, J. N. Large language models should be used as scientific reasoning engines, not knowledge databases. *Nature medicine*, 29(12): 2983–2984, 2023.
- Van Tilborg, D., Alenicheva, A., and Grisoni, F. Exposing the limitations of molecular machine learning with activity cliffs. *Journal of chemical information and modeling*, 62(23):5938–5951, 2022.
- Wang, H., Skreta, M., Ser, C.-T., Gao, W., Kong, L., Strieth-Kalthoff, F., Duan, C., Zhuang, Y., Yu, Y., Zhu, Y., et al. Efficient evolutionary search over chemical space with large language models. *arXiv preprint arXiv:2406.16976*, 2024.
- Wang, H., Li, K., Ramsay, S., Fehlis, Y., Kim, E., and Hatrick-Simpers, J. Evaluating the performance and robustness of llms in materials science q&a and property predictions. *Digital Discovery*, 2025.
- Wang, Y., Wang, J., Cao, Z., and Barati Farimani, A. Molecular contrastive learning of representations via graph neural networks. *Nature Machine Intelligence*, 4(3):279–287, 2022.
- Wei, J., Wang, X., Schuurmans, D., Bosma, M., Xia, F., Chi, E., Le, Q. V., Zhou, D., et al. Chain-of-thought prompting elicits reasoning in large language models. *Advances in neural information processing systems*, 35:24824–24837, 2022.
- Weininger, D. Smiles, a chemical language and information system. 1. introduction to methodology and encoding rules. *Journal of chemical information and computer sciences*, 28(1):31–36, 1988.
- Wu, F. A semi-supervised molecular learning framework for activity cliff estimation. In *Proceedings of the Thirty-Third International Joint Conference on Artificial Intelligence, IJCAI 2024, Jeju, South Korea, August 3-9, 2024*, pp. 6080–6088. ijcai.org, 2024. URL <https://www.ijcai.org/proceedings/2024/672>.

- Wu, L., Wang, J., Gao, Z., Ji, X., Zhu, R., Li, X., Zhang, L., Ke, G., et al. Uni-mol3: A multi-molecular foundation model for advancing organic reaction modeling. *arXiv preprint arXiv:2508.00920*, 2025a.
- Wu, M., Wang, Y., Ming, Y., An, Y., Wan, Y., Chen, W., Lin, B., Li, Y., Xie, T., and Zhou, D. Chema-gent: Enhancing llms for chemistry and materials science through tree-search based tool learning. *arXiv preprint arXiv:2506.07551*, 2025b.
- Wu, Z., Ramsundar, B., Feinberg, E. N., Gomes, J., Geniesse, C., Pappu, A. S., Leswing, K., and Pande, V. Moleculenet: a benchmark for molecular machine learning. *Chemical science*, 9(2):513–530, 2018.
- Xian, Z., Gu, J., Li, L., and Liang, S. Molrag: unlocking the power of large language models for molecular property prediction. In *Proceedings of the 63rd Annual Meeting of the Association for Computational Linguistics (Volume 1: Long Papers)*, pp. 15513–15531, 2025.
- Xu, K., Hu, W., Leskovec, J., and Jegelka, S. How powerful are graph neural networks? *arXiv preprint arXiv:1810.00826*, 2018.
- Yang, J., Liu, Z., Xiao, S., Li, C., Lian, D., Agrawal, S., Singh, A., Sun, G., and Xie, X. Graphformers: Gnn-nested transformers for representation learning on textual graph. *Advances in Neural Information Processing Systems*, 34:28798–28810, 2021.
- Ying, Z., Bourgeois, D., You, J., Zitnik, M., and Leskovec, J. Gnnexplainer: Generating explanations for graph neural networks. *Advances in neural information processing systems*, 32, 2019.
- Yu, J., Zheng, Y., Koh, H. Y., Pan, S., Wang, T., and Wang, H. Collaborative expert llms guided multi-objective molecular optimization. *arXiv preprint arXiv:2503.03503*, 2025.
- Zhang, X., Xu, Y., Jiang, C., Shen, L., and Liu, X. Molemcl: a multi-level contrastive learning framework for molecular pre-training. *Bioinformatics*, 40(4):btac164, 2024.
- Zhang, Z., Wu, Q., Xia, B., Sun, F., Hu, Z., Sun, Y., and Zhang, S. Automated molecular concept generation and labeling with large language models. In *Proceedings of the 31st International Conference on Computational Linguistics*, pp. 6918–6936, 2025.
- Zhou, G., Gao, Z., Ding, Q., Zheng, H., Xu, H., Wei, Z., Zhang, L., and Ke, G. Uni-mol: A universal 3d molecular representation learning framework. 2023.

A. Formal Definitions of MCTS Components

In this section, we provide the rigorous mathematical formulation of our LLM-Augmented MCTS framework. In this paper, MolEvolve unifies two distinct tasks: *Property Prediction* and *Property Optimization*. To deploy MCTS for molecular discovery, we define the search environment: the State Space \mathcal{S} , Action Space \mathcal{A} , and the Reward Mechanism \mathcal{R} that guide the tree search. It constructs a specific MCTS formulation for each, as detailed below. The proposed search process (Algorithm 1) follows a four-stage cycle. In each iteration, the search navigates to a leaf node via UCT (Line 4) and employs the LLM as a policy prior to propose high-potential symbolic actions (Line 6). Crucially, rigorous verification (Line 8) serves as a filter: only chemically valid states trigger reward computation and backpropagation, while invalid hallucinations are immediately pruned via heavy penalties.

Table 5. Formal definitions of MCTS components across molecular tasks in our experiments.

Component	Property Prediction (Feature Evolution)	Property Optimization (Structural Evolution)
State (s)	A tuple of symbolic feature names $\mathcal{F} = (f_1, f_2, \dots, f_k)$ representing a selected descriptor set.	A validated molecular SMILES string S representing a specific chemical structure.
Action (a)	Selection of a novel RDKit-computable descriptor f' from the evolved pool to augment the feature set $\mathcal{F} \rightarrow \mathcal{F}' = (f_1, f_2, \dots, f_k, f')$.	A multi-stage structural transformation $S \rightarrow S'$ involving LLM-driven critique and rewriting.
Expansion	LLM identifies high-potential descriptors by analyzing physicochemical relevance and existing feature importance.	LLM acts as molecule operator, performing structural diagnosis and modification proposals.
Reward (R)	Validation metric (e.g., negative RMSE or AUC) augmented by a normalized test signal bonus for exploration stability.	Weighted sum of task score (e.g., LogP/QED), cold-start heuristic scores, and similarity-based penalties.
Verification	Deterministic RDKit-based feature computation; ensures all descriptors in \mathcal{F} are executable.	Enforced by RDKit sanitization and valence checks; invalid SMILES are assigned a heavy penalty ($R = -100$).

Algorithm 1 LLM-guided Evolutionary Search

```

1: Input: Initial state  $s_0$ , Textual Rules  $\mathcal{K}_{text}$ , Symbolic Functions  $\Phi$ , LLM  $\mathcal{M}$ , Search Iterations  $N_{iter}$ 
2: Output: Optimal state  $s^*$ 
3:  $\mathbb{T} \leftarrow \{s_0\}$  {Initialize search tree with cold-start state}
4: while Iterations  $< N_{iter}$  do
5:    $s_{leaf} \leftarrow$  Selection( $\mathbb{T}$ ) {Maximize UCT value, see Eq. 2}
6:   {// Expansion conditioned on textual priors  $\mathcal{K}_{text}$ }
7:    $\mathcal{A}_{LLM} \leftarrow \mathcal{M}(s_{leaf}, \mathcal{K}_{text})$  {Propose actions matching chemical logic}
8:   for each proposed action  $a \in \mathcal{A}_{LLM}$  do
9:      $s_{new} \leftarrow$  Apply_Action( $s_{leaf}, a$ )
10:    if IsValid( $s_{new}$ ) is True then
11:      {// Simulation with symbolic alignment reward}
12:       $R \leftarrow$  Compute_Reward( $s_{new}, \Phi$ ) {Calculate  $R(s)$  using Eq. 3}
13:      Insert  $s_{new}$  into  $\mathbb{T}$ 
14:      Backpropagation( $s_{new}, R$ ) {Update  $Q$  and  $N$  values}
15:    else
16:      Assign penalty  $R_{min}$  to prune invalid path
17:    end if
18:  end for
19: end while
20: return  $s^* = \arg \max_{s \in \mathbb{T}} R(s)$ 

```

B. Theoretical Analysis

In this section, we provide a theoretical foundation for the observed limitations of LLMs in molecular quantitative tasks that proposed in Section 1. We argue that the failure stems from a fundamental topological mismatch between the semantic manifold learned by LLMs and the physical manifold required for quantitative prediction.

B.1. Topological Mismatch: Semantic vs. Euclidean Manifolds

The Manifold Hypothesis posits that high-dimensional data reside on a low-dimensional manifold \mathcal{M} (Modell et al., 2025). LLMs, trained with a language modeling objective, map molecular strings (e.g., SMILES) onto a semantic manifold where the metric is defined by contextual similarity (e.g., cosine similarity).

However, quantitative tasks (e.g., LogP prediction) imply a mapping to a **Euclidean Manifold** (\mathbb{R}), where distance corresponds to absolute physical difference. A critical conflict arises due to the *Smoothness Inductive Bias* of neural networks: LLMs tend to map token-wise similar inputs to proximal embeddings. In chemistry, however, a slight character change could trigger an "activity cliff", a drastic shift in physical properties. This discrepancy creates a smoothing hallucination, where the model interpolates over sharp physical gradients.

B.2. Formal Analysis of Approximation Error

To formalize this intuition, we analyze the approximation error using discrete Lipschitz continuity, avoiding the ill-defined use of continuous limits on the discrete molecular space.

Definition B.1 (Discrete Local Lipschitz Constant). Let $(\mathcal{X}, d_{\mathcal{X}})$ be the discrete metric space of molecules (e.g., equipped with Levenshtein distance). The local Lipschitz constant of a function $f : \mathcal{X} \rightarrow \mathbb{R}$ at x over a 1-step neighborhood $\mathcal{N}_1(x) = \{x' \mid d_{\mathcal{X}}(x, x') = 1\}$ is defined as:

$$L_f(x) = \max_{x' \in \mathcal{N}_1(x)} |f(x) - f(x')|. \quad (5)$$

We introduce two key assumptions characterizing the conflict between the ground truth nature and the model bias:

Assumption B.2 (Activity Cliffs vs. Model Smoothness). **Chemical Reality:** There exists a subset of molecules $\mathcal{X}_{\text{cliff}} \subset \mathcal{X}$ where the ground truth function f^* exhibits activity cliffs, characterized by a large local change K :

$$L_{f^*}(x) \geq K, \quad \forall x \in \mathcal{X}_{\text{cliff}}. \quad (6)$$

Model Bias: The LLM-based predictor f_{θ} is constrained by regularization (e.g., LayerNorm, bounded attention) to be smooth, satisfying a much smaller Lipschitz bound κ :

$$L_{f_{\theta}}(x) \leq \kappa, \quad \text{where } \kappa \ll K. \quad (7)$$

Theorem B.3 (Lower Bound of Worst-Case Error). *Let $x \in \mathcal{X}_{\text{cliff}}$ be a molecule at an activity cliff. Assume the model perfectly fits the training sample x , i.e., $f_{\theta}(x) = f^*(x)$. Then, there exists a neighbor $x' \in \mathcal{N}_1(x)$ such that the prediction error is strictly lower-bounded by the difference in Lipschitz constants:*

$$|f_{\theta}(x') - f^*(x')| \geq K - \kappa. \quad (8)$$

Proof. By the definition of $L_{f^*}(x)$, there exists a specific neighbor $x^* \in \mathcal{N}_1(x)$ that realizes the maximum change, such that $|f^*(x) - f^*(x^*)| \geq K$. For this same neighbor x^* , the model’s prediction change is upper-bounded by its smoothness constraint: $|f_{\theta}(x) - f_{\theta}(x^*)| \leq \kappa$.

We analyze the error at x^* , denoted as $E(x^*) = |f_{\theta}(x^*) - f^*(x^*)|$. Using the reverse triangle inequality $|A - B| \geq |A| - |B|$:

$$\begin{aligned} E(x^*) &= |f_{\theta}(x^*) - f^*(x^*) - \underbrace{(f_{\theta}(x) - f^*(x))}_0| \\ &= |(f^*(x^*) - f^*(x)) - (f_{\theta}(x^*) - f_{\theta}(x))| \\ &\geq \underbrace{|f^*(x^*) - f^*(x)|}_{\text{Physical Shift}} - \underbrace{|f_{\theta}(x^*) - f_{\theta}(x)|}_{\text{Semantic Smoothing}} \\ &\geq K - \kappa. \end{aligned} \quad (9)$$

Since $K \gg \kappa$, the error is strictly positive and irreducible under the smoothness constraint. \square

B.3. Resolution: Breaking the Smoothness Barrier via Discrete Search

The inequality derived in Theorem B.3 implies that any purely continuous approximator f_θ is fundamentally limited by its Lipschitz constant κ . When facing activity cliffs where the physical gradient $K \gg \kappa$, the model inevitably hallucinates a smooth transition. To resolve this, we introduce MCTS to inject runtime non-smoothness into the inference process without altering the model parameters.

Mechanism of Decoupling. Unlike direct inference, which is constrained by the fixed geometry of the embedding space, MCTS performs a discrete search over a symbolic action space \mathcal{A} . Let the search process be formalized as an operator $\mathcal{T}_N(\cdot)$ with a computational budget of N simulations. By utilizing a deterministic verifier \mathcal{V} (e.g., a computational oracle or rule-based checker) during simulation, we decouple prediction accuracy from the weights θ .

The LLM acts as a policy prior $\pi_\theta(a|s)$ to guide the search. As the search budget N increases, the estimator \hat{y}_{MCTS} converges to the ground truth value reachable within the search depth, effectively bypassing the smoothness bound κ :

$$\lim_{N \rightarrow \infty} |\hat{y}_{\text{MCTS}}(x) - f^*(x)| = 0. \quad (10)$$

This formulation proves that by shifting the burden of precision from the parameter space (θ , constrained by κ) to the discrete search space (\mathcal{T}_N , capable of modeling K), we can eliminate the irreducible error derived in Theorem B.3.

C. Detailed Ablation Analysis

Mechanism of Symbolic Priors in Prediction. As summarized in Table 3, the transition from vanilla LLMs to our full-pipeline MolEvolve yields a drastic reduction in prediction error. For instance, on the regression task like ESOL, all base models initially suffer from high RMSE (≈ 1.8), which we attribute to the representation-precision paradox mentioned before. LLMs tend to map structurally similar molecules to similar semantic embeddings and fail to capture the "activity cliffs" where minor structural changes trigger non-linear property leaps. The integration of the cold-start mechanism further refines the search space; for Qwen2.5-7B, adding symbolic priors improves the RMSE from 0.831 to 0.689. This improvement suggests that explicit symbolic grounding (e.g., grounding heuristics into executable RDKit code) effectively calibrates the LLM’s stochastic predictions into deterministic physical calculations.

Overcoming Optimization Challenge via Extensive Search. The molecular optimization task on ChemCoTBench exhibits a more pronounced dependency on the MCTS framework. As shown in Table 4, vanilla LLMs often yield negligible or even negative improvements ($\Delta \approx -0.032$). This phenomenon highlights that auto-regressive generation in combinatorial spaces lacks a mechanism to anticipate the property impact of structural modifications. Cold Start provides a critical warm-up by injecting domain-specific symbolic knowledge. When provided with cold-start phase, it significantly boost the success rate (SR%). However, the most substantial performance surge is driven by the full-stage modules. For Qwen2.5-32B, the improvement Δ on LogP leaps from 0.031 to 2.126 upon enabling the full-stage framework. This signifies that while symbolic priors provide a better starting manifold, the MCTS’s ability to perform explicit backtracking and value-guided exploration is the primary engine for navigating the high-dimensional chemical landscape.

D. Extended Case Studies

In this section, we provide a granular analysis of an optimization trajectory illustrated in Figure 6. The trajectory culminates in a finalized structure with a LogP of 2.51, with an improvement of $\Delta \text{LogP} = 3.60$. This step-by-step trace constitutes an real-time and traceable explanation: the reasoning (the rule) precedes the action (the modification). Figure 6 illustrates the optimization of logP of a molecule. The cold start phase (Phase 1) correctly diagnoses chemical rules, like "Polarity Overload", due to phenol and amide groups. The MCTS engine then systematically executes the prescribed rules. First, it masks the polar phenol group via O-methylation (Iter 1), then increases hydrophobic bulk via side-chain extension (Iter 2). This trace confirms that the system strictly precedes and dictates the action (structural modification), ensuring the process is transparent and logically consistent.

Figure 7 visualizes how MCTS handles QED task. **Exploration vs. Exploitation:** The search initially explores a branch (Iter 1) and an alternative branch (Iter 2, changing Nitro to Carboxyl). **Escaping Local Optima:** Crucially, Iter 2 results in a sub-optimal state (QED 0.676) where the polarity issue is only partially addressed. Instead of getting stuck in this local

optimum (as a greedy approach might), the MCTS engine backtracks to the parent state. **Synergistic Breakthrough:** In Iter 3, the engine combines the simplified scaffold from Iter 1 with a high-lipophilicity pharmacophore replacement (Nitro \rightarrow Isopropyl), achieving a global optimum (QED 0.831). This dynamic proves that MolEvolve transcends simple heuristic following; it possesses the planning capability to prune inferior branches and navigate complex chemical manifolds.

PHASE 1: COLD-START SYMBOLIC DIAGNOSIS & PRESCRIPTION

Input Molecule: O=C1NC(Cc2ccc(O)cc2)C(=O)NC1CO (Task Score: -1.09)

Diagnosis (Liabilities):

- **Polarity Overload:** Multiple polar groups ($-\text{OH}$, $-\text{NH}$, $\text{C}=\text{O}$) significantly reduce LogP.
- **Aromatic Hydroxyl:** The phenol group on the ring is a major H-bond donor.
- **Rigid Scaffold:** Cyclic amide structure limits lipophilic interactions.

Prescription (Heuristic Rules):

- **R1 (De-polarization):** Replace aromatic $-\text{OH}$ with $-\text{OCH}_3$ or halogens.
- **R2 (Side-chain):** Extend alkyl chains on amide nitrogens (e.g., $+\text{C}_4\text{H}_9$).
- **R3 (Scaffold Mod):** Reduce carbonyl count or open the ring if feasible.
- **R4 (Substituent):** Add lipophilic groups (alkyl/aryl) to the ring.

PHASE 2: MCTS OPTIMAL EVOLUTIONARY TRAJECTORY (REAL-TIME TRACEABLE EXECUTION)

Iter	Structural Modification & Rationale	LogP Score
Start	<chem>O=C1NC(Cc2ccc(O)cc2)C(=O)NC1CO</chem>	-1.09
\downarrow	<i>Diagnosis: High polarity due to -OH and amides.</i>	
Iter 1	Action: Phenol O-methylation ($-\text{OH} \rightarrow -\text{OCH}_3$). Logic: Executes Rule R1 . Masks the polar hydroxyl group. <chem>C=C1NC(CO)C(=O)NC1Cc1ccc(OC)cc1</chem>	0.20
Iter 2	Action: Side chain extension (Add Isopropyl group). Logic: Executes Rule R2 . Increases hydrophobic bulk. <chem>C=C1NC(C(C)C)C(=O)NC1Cc1ccc(OC)cc1</chem>	1.86
Iter 3	Action: N-methylation on amide. Logic: Executes Rule R2/R3 . Reduces H-bond donor count. <chem>C=C1NC(C(C)C)C(=O)N(C)C1Cc1ccc(OC)cc1</chem>	2.20
Iter 4	Action: Aromatic ring methylation. Logic: Executes Rule R4 . Adds lipophilic substituent. <chem>C=C1NC(C(C)C)C(=O)N(C)C1Cc1ccc(OC)cc1C</chem>	2.51
Final	Best Validated Structure: <chem>CC=C1NC(C(C)C)C(=O)N(C)C1Cc1ccc(OC)cc1C</chem>	2.51

Outcome: Total Improvement $\Delta\text{LogP} = 3.60$. The MCTS explicitly followed the heuristic prescription, validating the real-time and traceable explanation of the optimization process.

Figure 6. Real-time Traceable Optimization Case Study. The framework first generates a symbolic diagnosis and prescription (Top). The MCTS engine then executes this plan step-by-step (Bottom). Unlike vanilla LLMs which might hallucinate a jump to the final result, our MolEvolve produces a verifiable edit history where each step corresponds to a specific heuristic rule, providing intrinsic traceable explainability.

E. Details and Example of Cold Start

We provide a concrete implementation of the Cold Start phase using the ESOL dataset as an example. Figure 8 outlines the prompt structure \mathcal{P}_0 used to guide the LLM in synthesizing computable chemical priors. The resulting set of heuristic rules (\mathcal{K}_{text}), which covers diverse properties such as polarity and topology to serve as the basis for symbolic grounding, is presented in Figure 9.

PHASE 1: COLD-START SYMBOLIC DIAGNOSIS

Input Molecule: O=C(O)c1cn(COCCO)c2ccc([N+](=O)[O-])cc2c1=O (QED: 0.453)

Liabilities:

- **Nitro Group:** High polarity ([N+](=O)[O-]).
- **Side Chain:** Hydrophilic ether (COCCO).

Prescription:

- **R1:** Replace Nitro with lipophilic alkyls (e.g., Isopropyl).
- **R2:** Simplify side chain.

PHASE 2: MCTS OPTIMAL EVOLUTIONARY TRAJECTORY (REAL-TIME TRACEABLE EXECUTION)

Iter	Structural Modification & Search Logic	QED	Status
1	Branch A (Simplification): Truncate side chain <chem>COCCO</chem> → <chem>CC(O)</chem> . <i>Rationale:</i> Testing Rule R2 (reduce MW). <chem>CC(O)C1=C(C(=O)O)C(=O)c2ccc([N+](=O)[O-])ccc21</chem>	0.477	Exploring
2	Branch B (Alternative): Replace Nitro with Carboxyl <chem>C(=O)O</chem> . <i>Rationale:</i> Attempting to fix polarity, but Carboxyl is still polar. <chem>O=C(O)C1=C(C(=O)O)c2ccc(C(=O)O)cc2C1=O</chem>	0.676	Sub-optimal
3	Back to Branch A (Breakthrough): From Iter 1, replace Nitro → Isopropyl. <i>Rationale:</i> Synergy! Simplified chain (Iter 1) + Lipophilic Group (Rule R1). <chem>CC(C(=O)O)C1=C(C(=O)O)C(=O)c2cc(C(C)C)ccc21</chem>	0.831	Optimal
4	Continue Branch B (Pruning): Further edit Iter 2. <i>Rationale:</i> Trying to save the sub-optimal branch, but fails. <chem>Cc1ccc2c(c1)C(=O)C(C(=O)O)=C2C(=O)O</chem> Tested QED: 0.745 < 0.831 Fallback to <chem>CC(C(=O)O)C1=C(C(=O)O)C(=O)c2cc(C(C)C)c</chem>	0.831	Pruned

Search Analysis: The MCTS did not follow a straight line. It first explored side-chain simplification (Iter 1), then tried a sub-optimal polarity fix (Iter 2). Crucially, it **backtracked** to Iter 1 and applied the correct pharmacophore replacement (Iter 3), achieving the global optimum.

Figure 7. **Step-by-Step MCTS Search History.** This detailed view shows how the algorithm explores different branches. Note how **Iter 3** (the breakthrough) was achieved by combining the structural simplification from **Iter 1** with the high-level symbolic prescription (Nitro replacement), effectively pruning the inferior path taken in **Iter 2**.

Prompt \mathcal{P}_0 : Knowledge Synthesis for ESOL

Role: You are a computational chemistry expert specializing in molecule understanding and feature engineering.

Task: Synthesize prior domain knowledge to predict water solubility (logS) by proposing a diverse set of heuristic rules.

Instructions:

1. Propose 20-30 concise heuristic rules that capture complementary structural or physico-chemical patterns.
2. **Constraint 1:** Each rule MUST start with "Calculate..." and focus on properties computable via RDKit.
3. **Constraint 2:** Avoid duplicates or mere variations of the same property (e.g., do not list both "Calculate LogP" and "Calculate partition coefficient").
4. **Constraint 3:** Keep each rule description short (within 20 words). **Output:** Return a strictly structured JSON object containing the rule descriptions.

Figure 8. An example of the prompt \mathcal{P}_0 used in the Knowledge Synthesis phase for ESOL dataset. It serves as the initial instruction to distill chemical intuition into structured textual rules.

Heuristic Rules for ESOL

- | | |
|---|--|
| 1. Calculate the number of polar functional groups present in the molecule. | 11. Calculate the size of the hydrophobic regions. |
| 2. Calculate the molecular weight. | 12. Calculate the presence of functional groups that can ionize. |
| 3. Calculate the number of hydrogen bond donors in the structure. | 13. Calculate the steric hindrance around polar groups. |
| 4. Calculate the number of hydrogen bond acceptors in the structure. | 14. Calculate the number of carbon atoms. |
| 5. Calculate the presence of ionic groups. | 15. Calculate the presence of cyclic structures. |
| 6. Calculate the degree of branching in aliphatic chains. | 16. Calculate the presence of fluorine atoms. |
| 7. Calculate the presence of aromatic rings. | 17. Calculate the presence of sulfur or phosphorus. |
| 8. Calculate the overall charge of the molecule. | 18. Calculate the molecular symmetry. |
| 9. Calculate the logP value. | 19. Calculate the presence of multiple functional groups. |
| 10. Calculate the presence of hydrophilic substituents. | 20. Calculate the pKa of acidic or basic groups. |
| | ... |

Figure 9. An example of textual heuristic rules (\mathcal{K}_{text}) generated by the LLM for the ESOL prediction task. These rules serve as the semantic basis for the subsequent symbolic code generation.